ACS OMEGA

http://pubs.acs.org/journal/acsodf

Article

Exploring Arylazo-3,5-Bis(trifluoromethyl)pyrazole Switches

Bogdan C. Enache, Anamaria Hanganu, Cristina Tablet, Catalin C. Anghel, Codruta C. Popescu, Anca Paun, Niculina Daniela Hădade, Augustin M. Mădălan, and Mihaela Matache*

Cite This: *ACS Omega* 2022, 7, 39122−39135

Read Online

ACCESS | Metrics & More | Article Recommendations | Supporting Information

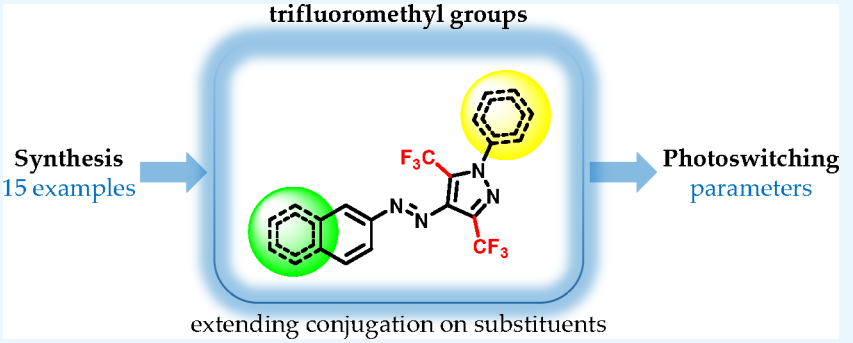

ABSTRACT: Arylazopyrazoles stand out among the azoheteroarene photoswitches due to their excellent properties in terms of stability of the least stable isomer and conversion between isomers, leading to their use in several interesting applications. We report herein the synthesis of arylazo-trifluoromethyl-substituted pyrazoles and their switching behavior under light irradiation. UV−vis and NMR experiments showed that arylazo-1*H*-3,5-bis(trifluoromethyl)pyrazoles displayed very long half-lives in DMSO (days), along with reasonable values of other parameters that characterize a photoswitch. Inclusion of naphthyl moieties as aryl counterparts of the arylazopyrazoles is beneficial only in combination with trifluoromethyl groups, while extending the conjugation by grafting the pyrazole moiety with electron-donating or -withdrawing substituents positively affects the photoswitching behavior, in terms of isomerization yield and half-lives of the least stable isomer. The experimental values were correlated with theoretical calculations indicating the valuable influence of the trifluoromethyl groups onto the photoswitching behavior.

INTRODUCTION

Photoswitches are defined as molecules that can reversibly convert between two states under the action of light.[1−7] The field had gained considerable attention in many scientific areas, from materials sciences to biological chemistry,[1−7] due to the tremendous advantage of light as a noninvasive stimulus, the simplicity of the molecular structures able to switch or the wide window of applications reported so far, from smart windows,[3] protective materials against sunlight, solar thermal fuels,[8] covalent organic frameworks (COFs),[9,10] data storage,[11−13] and controlled drug release or photopharmacology.[14,15] Besides the cyclization/ring-opening reaction (i.e., diarylethenes, spiropyrans/spirooxazines), the most common mechanism of photoswitching implies *E*−*Z* isomerization of double bonds. Thus, upon exposure to light, behavior of compounds containing C═C, C═N, and N═N (i.e., stilbenes, azobenzenes, imines, acylhydrazones, hemithioindigo) has been intensively studied, with each class showing their benefits and limitations.[1−7]

Azoheteroarenes represent a class of compounds developed as an alternative to azobenzenes in order to suppress major disadvantages, such as incomplete conversion between the isomers, caused by partial overlap of their absorption bands, or rather a short half-life of the least stable isomer. Nevertheless, development of azobenzene photoswitches chemistry has recently revealed interesting structures (i.e., 2,2′,6,6′-tetrafluoroazobenzene) that hold reasonable half-lives, almost quantitative switching conversion, and very well separated absorption bands.[16] The field of azoheteroarenes has also grown during the past decade, and since their first report,[17] numerous heterocycles[18,19] such as pyrole,[17,20] pyrazole,[17] imidazole,[21] indole,[22] and benzazole[23] were scanned for compatibility with photoswitching experiments indicating that each particular heterocycle brings novel features, prone to applications on a very wide scale.

Arylazopyrazoles are distinguished among the azoheteroarenes by displaying excellent properties associated with photoswitching behavior. Different unsubstituted or methyl-/dimethyl-substituted 3-, 4-, and 5-arylazopyrazoles,[17,24,25]

Received: August 4, 2022
Accepted: October 4, 2022
Published: October 20, 2022

https://doi.org/10.1021/acsomega.2c04984
ACS Omega 2022, 7, 39122−39135

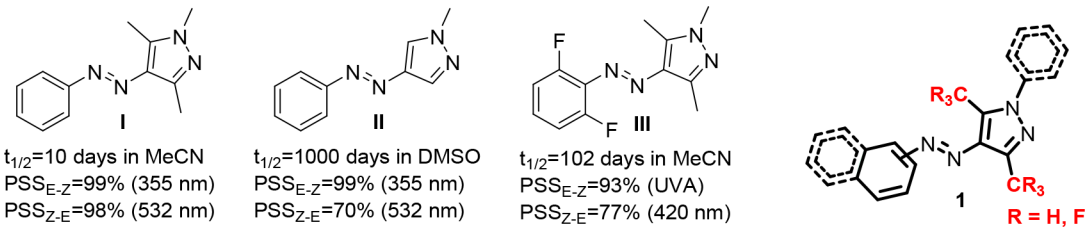

Figure 1. Examples of representative arylazopyrazoles (**I**, **II**, **III**) and the general structure of the compounds **1** prepared and investigated in this work.

either *N*-protected compounds[17,24,26] or N*H* derivatives,[27] were synthesized, and the effect of structural particularities over the photoswitching parameters has been reported. Thus, molecules containing N*H*-pyrazoles were found to be less effective as switches because of competing tautomerization processes, but they are strongly influenced by electronic effects provided by electron-donating or -withdrawing substituents on the aryl moiety.[27] At the same time, the presence of methyl groups on the heterocyclic moiety (structure **I** vs structure **II**, Figure 1) was found to accelerate the isomerization process.[17] Furthermore, dimethyl-substituted pyrazole-based azoheteroarenes of type **I** (Figure 1) were recognized for their suitability in biological applications, and slight structural modifications aiming to improve water solubility yielded photoswitches with appropriate properties, stability against glutathione[28] or utility for reversible control of DNA hybridization,[29] or as efficient enzyme inhibitors.[30,31] In addition, they were found to be useful in the construction of solar thermal fuels[32] or generation of hydrogels.[33,34]

Looking closer, arylazopyrazoles have not yet demonstrated their full capabilities in photoswitching experiments, and the search for novel compounds is still a topic of interest. The knowledge acquired so far regarding structural requirements was efficiently used in design, synthesis, and investigation of structures aimed to achieve better photoswitching parameters (structure **III**, Figure 1).

In this context, we report herein novel arylazopyrazoles of type **1** (Figure 1) and their behavior under light irradiation. In the design of these compounds, we targeted the investigation of the effects on the photoswitching parameters of (i) trifluoromethyl substituents grafted onto the pyrazole core, considering the remarkable properties that the fluorine atom has been proved to induce on the switching properties of azobenzene derivatives;[16,26] (ii) extended conjugated structures, brought by use of the naphthyl group, considering its rich electron nature and less studied properties in relation with photoswitches; and (iii) electronic effects of *N*-aromatic substituent of the pyrazole, with the use of both electron-donating and -withdrawing groups, taking into account the lack of systematic studies on this feature. Determination of the absorption properties, photostationary states, fatigue resistance, and thermal stability of the metastable isomer under irradiation indicated interesting behavior with respect to previously reported structures, with improvements in band separation for some of the synthesized compounds or thermal stability for others.

RESULTS AND DISCUSSION

Organic Synthesis. The synthetic approach we used for the preparation of target compounds **1** followed slightly modified previously described procedures (Scheme 1).[17,27,35,36]

Scheme 1. Synthesis of Compounds 1

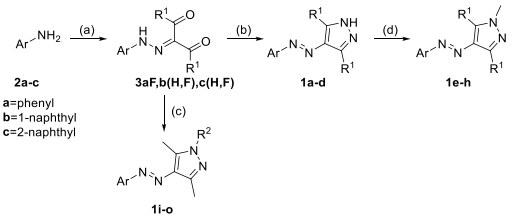

Reaction conditions: (a) $NaNO_2$, HCl, AcOH, then Hacac or Hfac, AcONa, EtOH, H_2O; (b) N_2H_4•H_2O, EtOH, rt or Δ; (c) R^2-$NHNH_2$ (or salt), EtOH, Δ; (d) MeI, KOH, H_2O, TBAB, rt (or DMSO, Δ);

Entry	Cmpn.	Ar	R^1	R^2	Yields (%)*
1.	**1a**	phenyl	CF_3	H	39**
2.	**1b**	1-naphthyl	CH_3	H	46**[27]
3.	**1c**	2-naphthyl	CH_3	H	46**
4.	**1d**	2-naphthyl	CF_3	H	24**
5.	**1e**	phenyl	CF_3	CH_3	19***
6.	**1f**	1-naphthyl	CH_3	CH_3	21***
7.	**1g**	2-naphthyl	CH_3	CH_3	25***
8.	**1h**	2-naphthyl	CF_3	CH_3	16***
9.	**1i**	1-naphthyl	CH_3	Ph	55**
10.	**1j**	1-naphthyl	CH_3	2,4-dinitrophenyl	37**
11.	**1k**	1-naphthyl	CH_3	4-tolyl	37**
12.	**1l**	2-naphthyl	CH_3	Ph	60**
13.	**1m**	2-naphthyl	CH_3	2,4-dinitrophenyl	39**
14.	**1n**	2-naphthyl	CH_3	4-tolyl	48**
15.	**1o**	2-naphthyl	CH_3	2-naphthyl	54**
16.	**3aF**	phenyl	CF_3	-	54
17.	**3bH**	1-naphthyl	CH_3	-	76[27]
18.	**3bF**	1-naphthyl	CF_3	-	40
19.	**3cH**	2-naphthyl	CH_3	-	71[28]
20.	**3cF**	2-naphthyl	CF_3	-	58

* *Isolated;* ** *after two steps;* *** *after three steps;*

*Isolated **after two steps ***after three steps

Thus, diazotization of primary aromatic amines **2a−c** at low temperature was followed by condensation with acetylacetone (Hacac) or hexafluoroacetylacetone (Hfac) to yield hydrazones **3**. These were subjected to reactions with hydrazine hydrate to yield compounds **1a−d** or with substituted aromatic hydrazines (or their salts) to yield compounds **1i−o**. Further, *N*-alkylation of the resulted pyrazoles **1a−d** with methyl iodide in a basic medium furnished target products **1e−h**. The overall yields after two or three steps indicated good accessibility to these compounds (Scheme 1).

Structural Analysis. Each synthetic step was accompanied by thorough characterization of the resulting product. Thus, a notable feature of hydrazones **3bH** and **3cH** was the magnetic

https://doi.org/10.1021/acsomega.2c04984
ACS Omega 2022, 7, 39122−39135

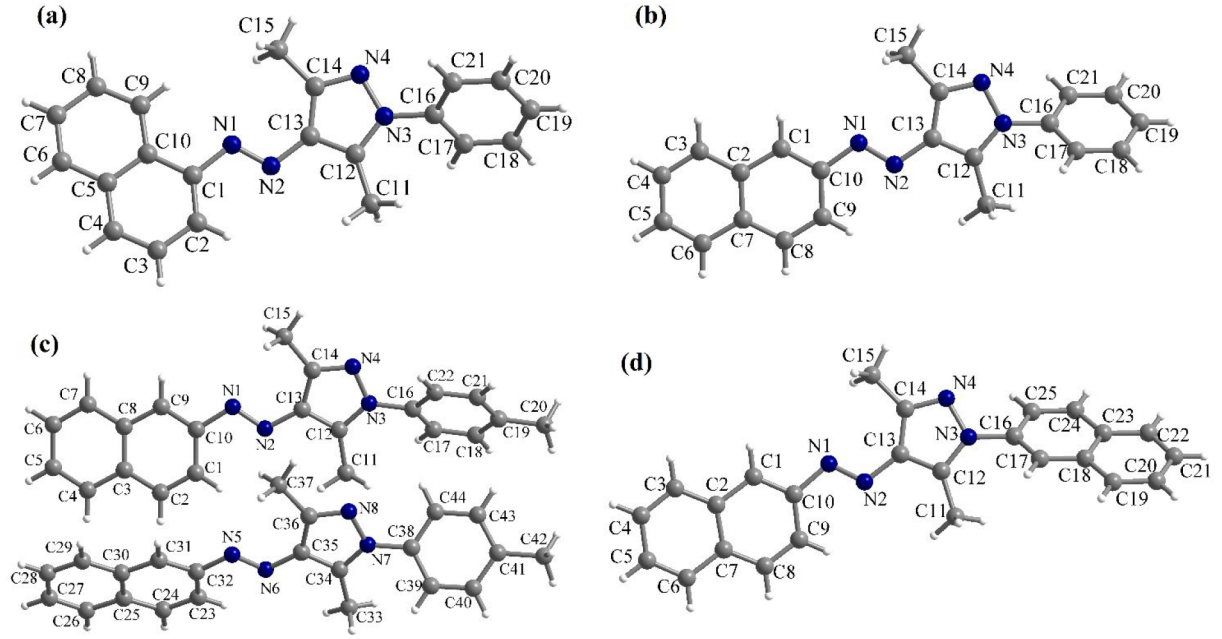

Figure 2. Molecular structures of compounds **1i** (a), **1l** (b), **1n** (c), and **1o** (d) revealed by single-crystal X-ray diffraction.

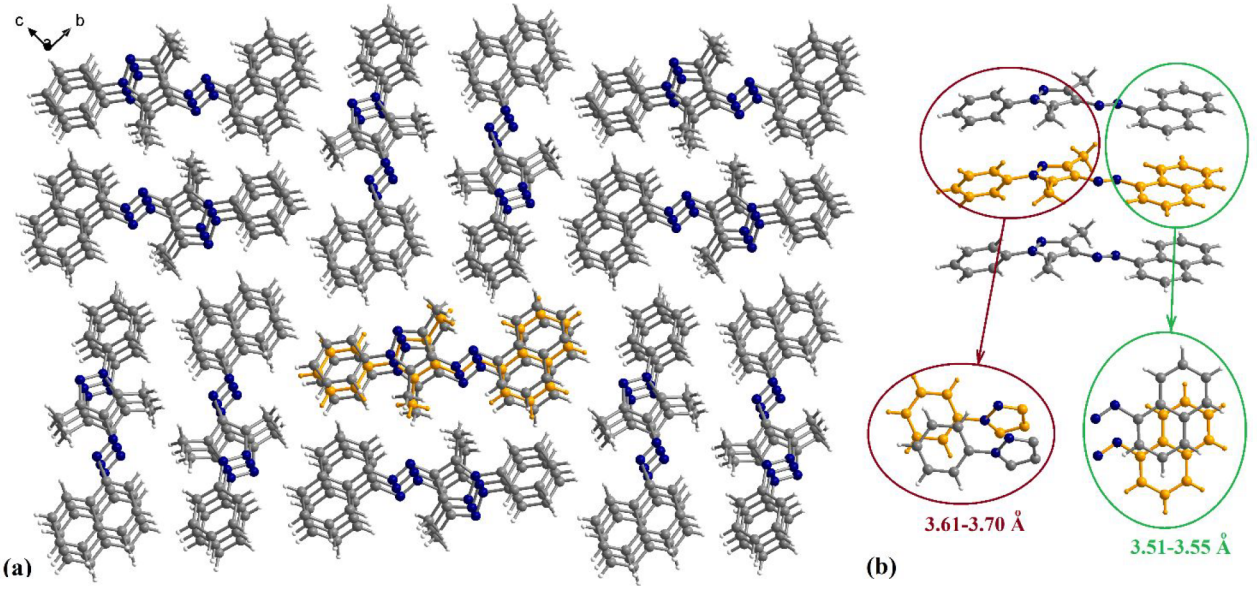

Figure 3. View along the crystallographic *a* axis of the packing diagram of crystal **1i** (a) and details of the $\pi-\pi$ interactions established between neighboring molecules within a supramolecular column (b).

nonequivalence of the methyl groups observed in ^{1}H NMR spectra (see Supporting Information). This behavior and quite a few studies to elucidate it have been previously described. For example, earlier,[37] the cause was attributed to the existing N−H···O═C intramolecular hydrogen bond, as inferred by IR spectra,[37] which was also sustained by large chemical shift of the N*H* in ^{1}H NMR spectra.[37] Later,[38,39] studies involving X-ray diffraction or computational analysis confirmed this assumption. Although we observed in the solid state formation of the intramolecular hydrogen bond (see Supporting Information for single-crystal X-ray diffraction of **3bH** and **3cF**), we have also performed NMR experiments. We ran ^{1}H NMR spectra in various solvents, showing distinct signals corresponding to the methyl groups at δ = 2.69, 2.57 ($CDCl_3$), 2.55, 2.45 (DMSO-d_6), and 2.58, 2.48 (MeCN-d_3) ppm, respectively and a strongly deshielded signal for N*H* at δ = 15.74 ($CDCl_3$), 15.31 (DMSO-d_6), and 15.48 (MeCN-d_3) ppm (see Supporting Information). VT-NMR experiments performed in DMSO-d_6 and MeCN-d_3 indicated deshielding of the signals corresponding to the methyl protons; however, up to 330 K, no coalescence could be observed. Addition of D_2O led to deuterium exchange and the disappearance from the spectrum of the signal corresponding to N*H*; however, the signals corresponding to the methyl groups only suffered shielding. An increase of temperature also led to deshielding of the signals, with the two methyl groups preserving the nonequivalent character. All of these suggested a restricted rotation around N−N and N−C bonds that avoids interchange of different conformation and the highest stability of the conformation that is able to form an intramolecular hydrogen

https://doi.org/10.1021/acsomega.2c04984
ACS Omega 2022, 7, 39122−39135

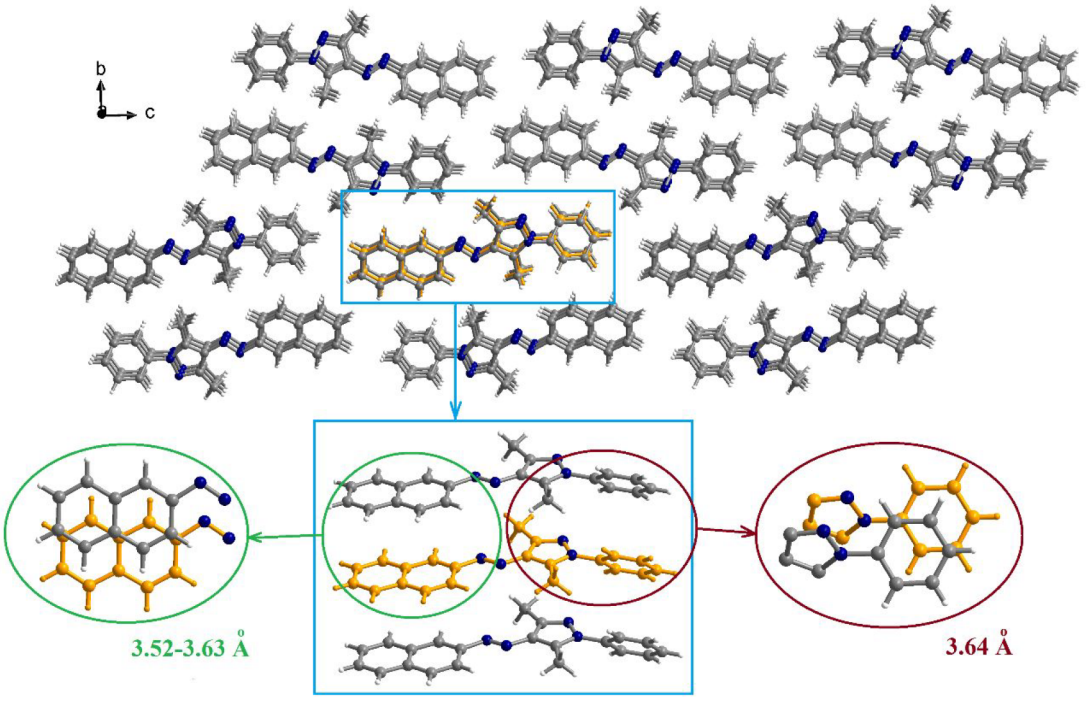

Figure 4. View of the packing diagram in **1l** along the crystallographic *a* axis. The insets show details of the $\pi-\pi$ interactions established between the molecules along the crystallographic *a* axis.

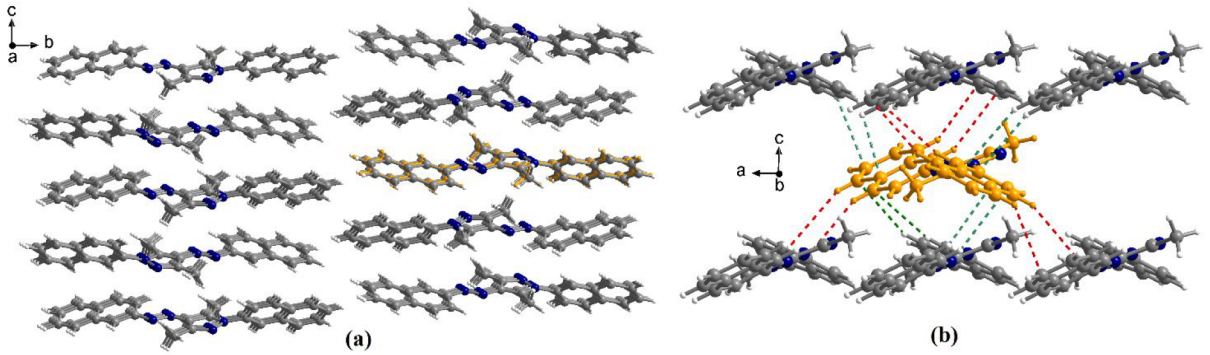

Figure 5. View of the packing diagram in crystal **1o** along the crystallographic *a* axis (a) and details of the CH$-\pi$ interactions in the crystallographic *ac* plane (b).

bond. For fluorine derivatives, the signal corresponding to N*H* was also very deshielded (i.e., at δ = 14.75 ppm for **3cF**, see Supporting Information). ^{19}F NMR spectra indicated negative values of the chemical shifts, different for the two trifluoromethyl groups (around δ = −68 ppm/ δ = −83 ppm, see Supporting Information).

Moving forward to the target arylazopyrazoles, suitable crystals of compounds **1i**, **1l**, **1n**, and **1o** for single-crystal X-ray diffraction were obtained by slow evaporation from diisopropylether or toluene. Cooling supersaturated DMSO solutions was also efficiently used as a crystallization technique. The molecular structures of the compounds **1i**, **1l**, **1n**, and **1o** are presented in Figure 2.

Compounds **1i** (Figure 2a), **1l** (Figure 2b), and **1o** (Figure 2d) crystallize in monoclinic space groups: $P2_1/n$ (**1i**) and $P2_1/c$ (**1l** and **1o**). Compound **1n** (Figure 2c) crystallizes in the $P\bar{1}$ triclinic space group, and the asymmetric unit contains two molecules.

The analysis of molecular structures revealed similar conformations for the fragments containing the naphthyl and pyrazole moieties linked by the azo group. These fragments are almost coplanar for compounds **1i**, **1l**, and **1o**, with dihedral angles defined by the mean planes of naphthyl and pyrazole rings of 7.9° (**1i**), 4.8° (**1l**), and 9.3° (**1o**). The two crystallographic independent molecules of compound **1n** present larger dihedral angles between the mean planes of naphthyl and pyrazole rings, both with values around 22°.

In all cases, there is a significant deviation from coplanarity for the aromatic fragments bonded to the N3 atom of the pyrazole ring, most probably because the methyl groups on the pyrazole ring create a steric effect. The values of the dihedral angles between the mean planes of the aromatic fragments connected to the N3 (or N7 in **1n**) atom and of the pyrazole rings are 50.4° (**1i**), 47.6° (**1l**), 36.2°, and 33.4° (**1n**), and, respectively, 45.7° (**1o**).

The analysis of the packing diagram for **1i** shows the organization of the molecules in piles running along the crystallographic *a* axis (Figure 3). These supramolecular columns are formed through $\pi-\pi$ interactions established mostly between the naphthyl fragments of neighboring

https://doi.org/10.1021/acsomega.2c04984
ACS Omega 2022, 7, 39122−39135

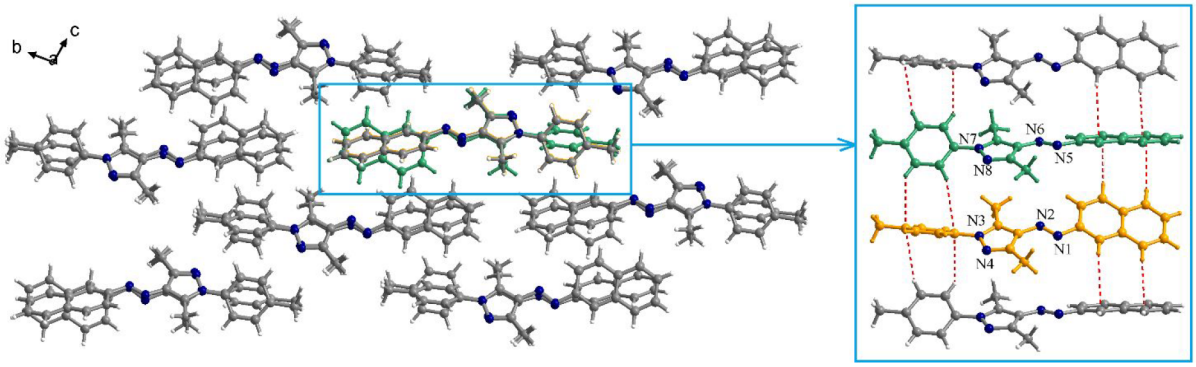

Figure 6. View of the packing diagram in crystal **1n** along the crystallographic *a* axis and details of the CH−π interactions established within a supramolecular column.

Table 1. UV−vis Absorption Maxima of *E* and *Z* Isomers (DMSO)

					λ_{max} (nm) ($\varepsilon \times 10^4$ M^{-1} cm^{-1})					
					$\pi-\pi^*$			n−π^*		
entry	compd	Ar	R^1	R^2	*E*	*Z*	$\Delta\lambda$	*E*	*Z*	$\Delta\lambda$
1	-[17]	phenyl	CH_3	H	330	293	−37	421	436	15
2	-[27]	phenyl	CH_3	CH_3	335	296	−39	425	441	16
3	**1a**	phenyl	CF_3	H	344 (1.27)	274	−70	424 (0.967)	440	16
4	**1b**	1-naphthyl	CH_3	H	372 (1.95)	297	−75	390 (1.57)	448	55
5	**1c**	2-naphthyl	CH_3	H	345 (2.57)	296	−49	380 (1.36)	443	63
6	**1d**	2-naphthyl	CF_3	H	347 (1.85)	313	−34	384 (1.18)	430	46
7	**1e**	phenyl	CF_3	CH_3	320 (1.71)	284	−36	428 (0.695)	423	−5
8	**1f**	1-naphthyl	CH_3	CH_3	373 (1.87)	323	−50	398 (1.76)	450	52
9	**1g**	2-naphthyl	CH_3	CH_3	348 (2.22)	300	−48	378 (1.32)	447	69
10	**1h**	2-naphthyl	CF_3	CH_3	332 (1.72)	316	−16	400 (0.468)	434	34
11	**1i**	1-naphthyl	CH_3	Ph	377 (1.64)	317	−60	400 (1.26)	451	51
12	**1j**	1-naphthyl	CH_3	2,4-dinitrophenyl	380 (2.12)	321	−59	410 (1.45)	452	42
13	**1k**	1-naphthyl	CH_3	4-tolyl	376 (1.98)	322	−54	404 (1.39)	455	51
14	**1l**	2-naphthyl	CH_3	Ph	350 (2.35)	307	−43	380 (1.50)	450	70
15	**1m**	2-naphthyl	CH_3	2,4-dinitrophenyl	344 (3.02)	312	−32	379 (2.28)	436	57
16	**1n**	2-naphthyl	CH_3	4-tolyl	353 (2.75)	315	−40	380 (1.97)	450	70
17	**1o**	2-naphthyl	CH_3	2-naphthyl	357 (3.15)	316	−41	381 (2.35)	446	65

molecules, with separation between them in the range 3.51−3.55 Å, but also between neighboring phenyl fragments, with a separation between 3.61 and 3.70 Å. The overlapping patterns are presented in the insets of Figure 3b. In the crystallographic *bc* plane, the molecules are ordered in centrosymmetric pairs with two different orientations of the long axis of the molecule.

Compound **1l** is also organized in supramolecular columns following the crystallographic *a* axis through $\pi-\pi$ interactions (Figure 4). The distances between the naphthyl fragments range between 3.52 and 3.63 Å, while for phenyl fragments the separation is approximately 3.64 Å. All molecules lie with the long axis of the molecule on the crystallographic *c* axis.

In the case of compound **1o** (Figure 5a), packing is ruled by CH−π interactions, which generate a 2D supramolecular architecture in the crystallographic *ac* plane (Figure 5b). Each molecule interacts with six other neighboring molecules as a donor (red dotted lines) or acceptor (green dotted lines). The distances for the CH−π interactions are 2.9−3.25 Å.

The analysis of the packing motif in **1n** (Figure 6) shows the formation of supramolecular columns through CH−π interactions established between the naphthyl moieties and tolyl fragments, respectively (Figure 6). The CH−π contacts within the supramolecular columns are 2.85−3.26 Å. In each column, the two crystallographic types of molecules alternate (the two types were labeled with orange and green, respectively). The naphthyl fragments of the molecules containing the nitrogen atoms N5−N8 (labeled with green) are also involved in CH−π interactions with naphthyl fragments of the molecules from neighboring columns (2.80 Å).

Photoswitching Experiments. Once the compounds were synthesized and characterized, we focused on photoswitching experiments that were monitored by NMR or UV−vis spectroscopy. Solutions of compounds **1** in DMSO (varying from 5 μM to 70 μM) were first investigated by UV−vis spectroscopy to determine absorption maxima and molecular extinction coefficients of *E* isomers, and the results are summarized in Table 1 (full UV−vis spectra and detailed calculation for molecular extinction coefficients are found in Supporting Information). The extinction coefficients vary between 1.64×10^4 M^{-1} cm^{-1} and 3.15×10^4 M^{-1} cm^{-1} at the absorption maximum corresponding to the $\pi-\pi^*$ transition and lower for the absorption maximum corresponding to the n−π^* transition (Table 1 and Supporting Information). Before irradiations, all compounds were thermally adapted (heating at 90 °C) to ensure the equilibrium was shifted toward the *E* isomer.

https://doi.org/10.1021/acsomega.2c04984
ACS Omega 2022, 7, 39122−39135

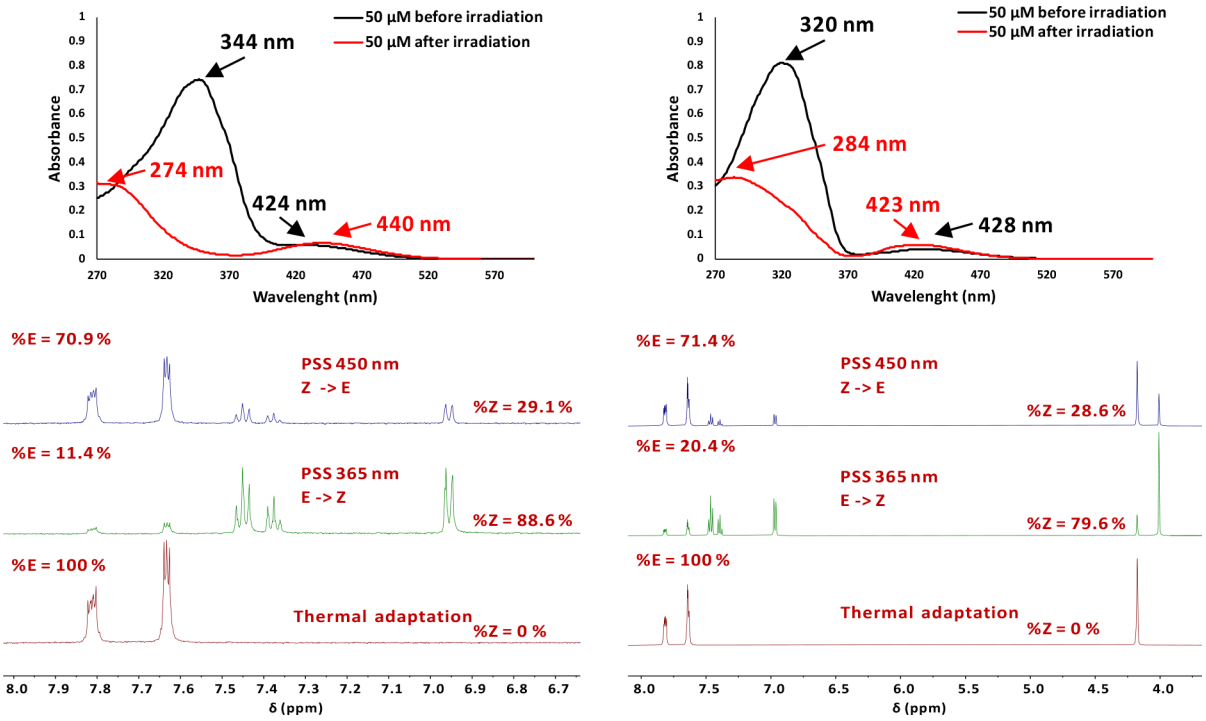

Figure 7. (Top left) UV−vis spectrum of **1a**. (Top right) UV−vis spectrum of **1e**. (Bottom left) NMR spectra (fragments) for compound **1a** before irradiation, after irradiation at 365 nm, and after irradiation at 450 nm. (Bottom right) NMR spectra (fragments) for compound **1e** before irradiation, after irradiation at 365 nm, and after irradiation at 450 nm.

Table 2. Photostationary States (*Z*%) and Determined Half-Lives of the Least Stable Isomer

entry	compd	Ar	R^1	R^2	PSS (*Z*%)	$t_{1/2}$
1	**1a**	phenyl	CF_3	H	88.6	∼22 days
2	**1b**	1-naphthyl	CH_3	H	-	*a*
3	**1c**	2-naphthyl	CH_3	H	90.9	1.5 h
4	**1d**	2-naphthyl	CF_3	H	82.0	∼10 days
5	**1e**	phenyl	CF_3	CH_3	79.6	∼146 days
6	**1f**	1-naphthyl	CH_3	CH_3	89.3	13.1 h
7	**1g**	2-naphthyl	CH_3	CH_3	94.3	52.5 h
8	**1h**	2-naphthyl	CF_3	CH_3	76.3	∼78 days
9	**1i**	1-naphthyl	CH_3	Ph	84.9	9.5 h
10	**1j**	1-naphthyl	CH_3	2,4-dinitrophenyl	34.2	9.4 h
11	**1k**	1-naphthyl	CH_3	4-tolyl	53.3	9.5 h
12	**1l**	2-naphthyl	CH_3	Ph	92.2	59.8 h
13	**1m**	2-naphthyl	CH_3	2,4-dinitrophenyl	32.9	70.7 h
14	**1n**	2-naphthyl	CH_3	4-tolyl	91.5	44.4 h
15	**1o**	2-naphthyl	CH_3	2-naphthyl	49.0	46.8 h

[a]Could not be determined due to very fast thermal back-isomerization.

Trifluoromethyl-Substituted Pyrazoles. Compounds **1a** and **1e**, bearing trifluoromethyl groups, displayed in the UV−vis spectra, recorded before irradiation, similar profiles with the corresponding dimethyl-substituted compounds[17,24,27] (Table 1, entries 1 and 2), with slightly shifted maxima at λ_{max} = 344 nm for **1a** (red-shift) and λ_{max} = 320 nm for **1e** (blue-shift) for $\pi-\pi^*$ transition. The $n-\pi^*$ band is clearly visible in both cases at λ_{max} = 424 nm and λ_{max} = 428 nm. Irradiation of DMSO solutions led to changes both in UV−vis (50 μM) and NMR (1.5 mM) spectra (Figure 7). Thus, we noticed a blue-shift of the $\pi-\pi^*$ absorption band corresponding to the *Z* isomer (λ_{max} = 274 nm for **1a** and λ_{max} = 284 nm for **1e**), while the $n-\pi^*$ band suffered a red-shift to λ_{max} = 440 nm for **1a** and a blue-shift to λ_{max} = 423 nm for **1e**; thus, there was very good $\pi-\pi^*$ band separation for both compounds and lower $n-\pi^*$ band separation for the *N*-methyl-substituted pyrazole **1e**. Notably, we could follow both photochemical isomerization processes (i.e., irradiation at λ_{max} = 365 nm and λ_{max} = 450 nm) by NMR, and the obtained values of the photostationary states (PSS) were higher than 70% (see Table 2 and Figure 7). More interestingly, we determined very long half-lives of the metastable isomers, in the range of days (∼22 days for **1a** and 146 days for **1e**, see Table 2), values considerably higher than for the corresponding, previously reported, methyl-substituted derivatives (approximately 8 h for the N*H*-pyrazole and 10 days for the *N*-methyl pyrazole in MeCN).[17,24,27]

https://doi.org/10.1021/acsomega.2c04984
ACS Omega 2022, 7, 39122−39135

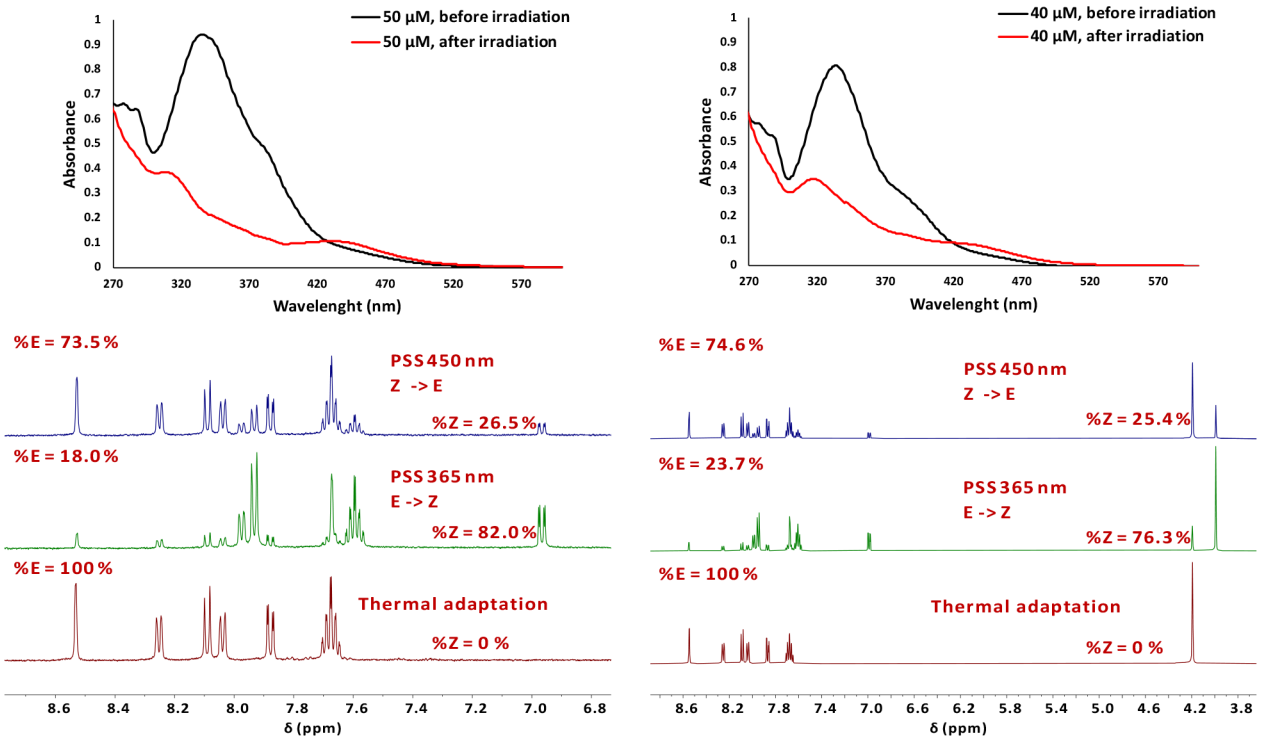

Figure 8. (Top left) UV−vis spectra of **1d** before and after irradiation at 365 nm. (Top right) UV−vis spectra of **1h** before and after irradiation at 365 nm. (Bottom left) NMR spectra for compound **1d** before irradiation, after irradiation at 365 nm, and after irradiation at 450 nm. (Bottom right) NMR spectra for compound **1h** before irradiation, after irradiation at 365 nm, and after irradiation at 450 nm.

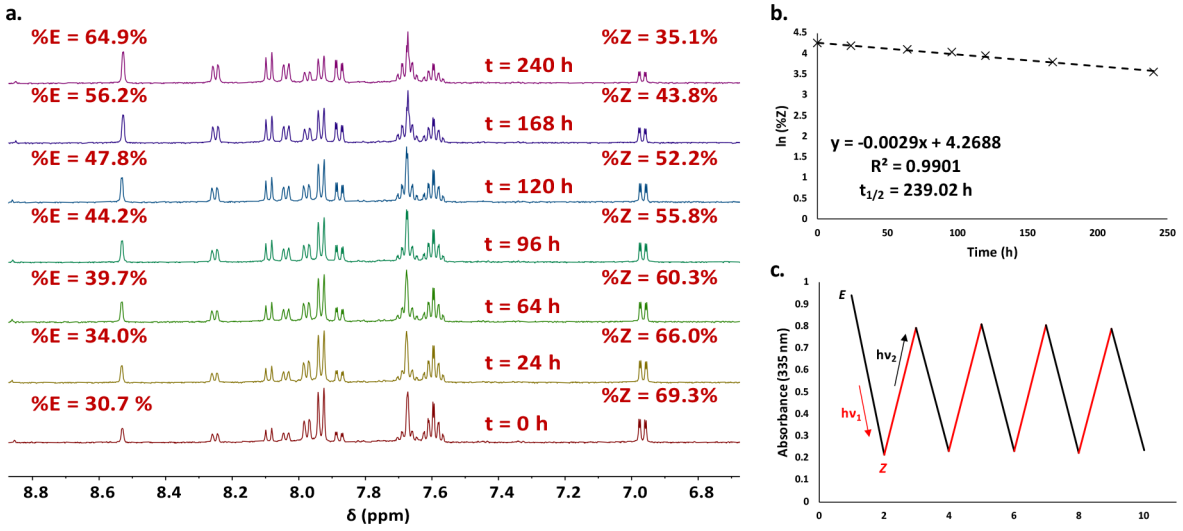

Figure 9. (a) Thermal back-isomerization of **1d**, monitored using ^{1}H NMR in DMSO-d_6. (b) Half-life determination of **1d** in DMSO-d_6. (c) Fatigue study of **1d** in DMSO through irradiation cycles at 365 and 450 nm.

Fluorine has been reported as a very important substituent in the design of efficient and functional photoswitches, both for azobenzenes[16] and heteroarenes on the aryl side (Figure 1, compound **III**),[26] with breakthroughs both on the separation of the absorption bands of the two isomers (very long red-shift of the n−π* of the *Z* isomer) and half-lives of the metastable isomer. The influence of fluorine has been rationalized, mostly using computational analysis, by a sum of effects, especially the stabilization of the n orbital of the *Z* isomer.[16] On the other hand, long half-lives in the heteroarene series were shown to be the consequence of a T-like shaped structure of the *Z* isomer, resulting from a C−H···π interaction for nonsubstituted heterocycles like pyrrole or pyrazole.[24] However, for alkyl-substituted azoheteroarenes like compound **I** (Figure 1), such a conformation is disfavored, and a twisted conformation was calculated to be more reasonable. Thus, in this case, stabilization of the *Z* isomer was proposed to be due to dispersive effects, which prevail in any eventual bulky clashes.[24] The trifluoromethyl group in our compounds appears to act as a stabilizing element, especially for the N*H* derivatives, for which the switching parameters were obviously improved. This was also supported by compounds **1d** and **1h**, which resulted from replacement of the phenyl group with 2-naphthyl moiety (Figure 8, Table 2). For comparison purposes, we prepared the

https://doi.org/10.1021/acsomega.2c04984
ACS Omega 2022, 7, 39122−39135

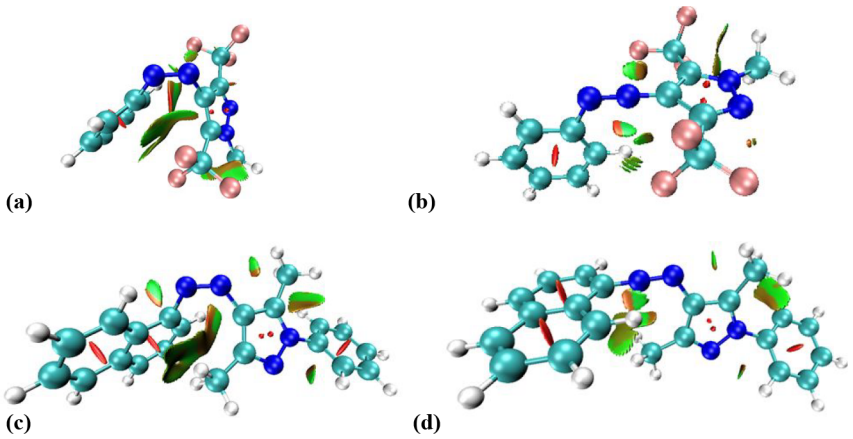

Figure 10. Calculated NCI surfaces for isomer (*Z*) and transition states (TSs) of azopyrazoles **1e** (**a**, **b**) and **1i** (**c**, **d**). Attractive dispersive intramolecular effects are marked by green surface, whereas repulsive ones are marked by a red surface.

corresponding dimethyl-substituted pyrazoles **1c** and **1g**. We could observe a poor separation of the absorption bands, as previously observed for naphthyl derivatives[27] with no significant shifts in the absorption maxima for N*H*-compounds **1d** and **1c** and better responses of the *N*-methyl **1h** and **1g** (Table 1). Interestingly, compound **1h** displayed a lower absorption maximum (λ_{max} = 332 nm), almost similar to the parent arylazopyrazole **I** (λ_{max} = 335 nm), bearing a phenyl group.[24]

However, a very large enhancement of the half-lives, of about 10 days for compound **1d** (compared to 1.5 h for **1c**) and ∼134 days for compound **1h** (compared to ∼2.35 days for compound **1g**), was determined from data obtained by irradiation and NMR monitoring of the back-isomerization process at room temperature (Figure 9), which are the highest values reported so far for N*H*-azopyrazoles.[25,27] While for the *N*-methyl-substituted compounds the isomerization process is clear and the influence of the trifluoromethyl groups resulted in stabilization of the least stable isomer, in the case of the N*H*-substituted pyrazoles, tautomerization could be a competitive process for the N═N isomerization bond.[25,27] However, it is very unlikely that the tautomerization may occur in this case, and this was also suggested by theoretical calculations (*vide infra*).

The trifluoromethylated compounds displayed lower, but reasonable, PSS values as compared to those of the corresponding methyl-substituted pyrazoles when *E*−*Z* and *Z*−*E* isomerizations were performed photochemically (**1d** 73.5% for *E*, and 82.0% for *Z*; **1h** 74.6% for *E*, and 76.3% for *Z*).

We have also obtained ^{19}F NMR spectra for the trifluoromethyl-substituted pyrazoles, before and after irradiation, and we noticed, for each *E* and *Z* isomer, two ^{19}F NMR peaks (negative values around δ = −60 ppm, see Supporting Information for full spectra), with peak separations of Δ = 0.25 ppm or greater that could afford accurate integration for determination of *E*/*Z* ratios.

Extended-Conjugated Pyrazoles. The absorption spectra corresponding to the *E* isomers of compounds containing naphthyl moiety revealed a clear π−π* absorption band with maxima between λ_{max} = 372 nm and λ_{max} = 376 nm for compounds bearing 1-naphthyl substituent and are slightly blue-shifted, with maxima between λ_{max} = 345 nm and λ_{max} = 357 nm, for compounds bearing 2-naphthyl moiety (Table 1 and Supporting Information).

Irradiation of the compounds at λ_{max} = 365 nm led to a change in the absorption profile, corresponding to formation of the *Z* isomer: the band assigned to the π−π* transition was blue-shifted with maxima between λ_{max} = 317 nm and λ_{max} = 323 nm for compounds bearing 1-naphthyl moiety and maxima between λ_{max} = 300 nm and λ_{max} = 316 nm for compounds bearing 2-naphthyl moiety; on the other hand, a clear intensification of the red-shifted band assigned to the n−π* transition was observed with maxima between λ_{max} = 448 nm and λ_{max} = 455 nm for compounds bearing 1-naphthyl substituent and maxima between λ_{max} = 430 nm and λ_{max} = 450 nm for compounds bearing 2-naphthyl moiety.

Thus, one can note a very good addressability of the synthesized compounds, with differences in the absorption maxima between the two isomers, corresponding to an n−π* transition ranging between $\Delta\lambda_{max}$ = 42 and $\Delta\lambda_{max}$ = 70 nm. A notably different result was provided by behavior of compounds **1a** and **1d** compared to **1b** and 1-naphthyl derivative **1c**.[17] The arylazo-1*H*-3,5-dimethylpyrazoles were systematically investigated to show the influence of electronic and steric effects of aryl substituents as well as the influence of hydrogen bonding, concentration, and solvent on *Z* isomer stability, indicating a complex interplay between all of these factors. In our case, the presence of the fluorine atoms probably prevails over the cumulated factors previously reported. In the case of the *N*-methylated derivatives, the fluorine compound **1h** showed a lower separation of the absorption bands and PSS values compared to the methyl-substituted **1g**, but with a much longer half-life.

Finally, extending the conjugation of the pyrazole, by *N*-substitution with various aryl groups, yielded particular features for each photoswitching parameter. The profile of the absorption bands before and after irradiation did not significantly change compared to the *N*-methyl derivatives **1g** and **1f**, and the absorption maxima varied around λ_{max} = 373 nm and λ_{max} = 398 nm for the *E* isomer and λ_{max} = 323 nm and λ_{max} = 450 nm for the *Z* isomer, except for compounds bearing the 2-naphthyl moiety and *N*-phenyl or *N*-tolyl groups **1l** and **1n**, for which n−π* band separation could be observed between the two isomers. In addition, the 2-naphthyl derivatives generally yielded enhanced PSS values for the *Z* isomer (>90%), especially in the case of the phenyl and *p*-tolyl

https://doi.org/10.1021/acsomega.2c04984
ACS Omega 2022, 7, 39122−39135

derivatives **1l** and **1n**, similar to the *N*-methyl-substituted **1g**, while the derivatives containing electron-withdrawing substituents or a bulkier naphthyl showed lower isomerization yields, most likely due to steric effects. The corresponding 1-naphthyl derivatives were most likely affected by steric effects in completing the isomerization. However, better results could be observed in terms of half-lives. The derivatives containing the 2-naphthyl moieties led to values in the range of days (Table 2), while the stability of the 1-naphthyl compounds was shown to be in the range of hours. Interestingly, compound **1m** showed the longest half-life among the 2-naphthyl derivatives, suggesting that electron-withdrawing substituents had a significant influence on the stabilization of the less stable isomer. In corroboration with the results obtained for the trifluoromethyl derivatives, one could establish that the electronic effects play indeed a major role in the behavior of such compounds, under light irradiation.

Experiments of repeated isomerization and back-isomerization, both photochemically and thermally, were performed and monitored by NMR or UV−vis spectroscopy in order to verify the fatigue resistance of the novel synthesized compounds, and these indicated that they are stable to repeated exposure of light (at least 5 cycles, see Supporting Information).

Theoretical Calculations. In order to get a closer insight into the intriguing high stability of some arylazopyrazole derivatives, we performed theoretical calculations for compounds **1e** and **1i**, using ωB97XD/6-31+G**[40,41] (see Supporting Information for details), as the most representative among all our compounds. We initially optimized the lowest-energy conformers for *E*, *Z*, and transition state (TS) forms (Table S7 and Figures S65−S66 in Supporting Information show their energies and geometries), in the gas phase, considering previous findings for similar compounds regarding the negligible effect of the solvent on the computed relative energy barriers.[24] *Z* isomers display a *twisted* conformation,[17,24] due to the bulky nature of methyl and trifluoromethyl groups. The noncovalent interaction (NCI) surfaces (Figure 10) indicated a sum of stabilizing dispersive effects between the aryl fragments and methyl and trifluoromethyl groups, respectively.

According to previous reports, there were two possible isomerization pathways for azobenzenes,[42] i.e., rotation by changing the CNNC dihedral angle, or inversion by varying the C−N═N angle, and therefore we performed surface scan calculations to identify which mechanism was most likely to occur in our case (Figure 11). The results showed that *Z*−*E* isomerization followed an inversion mechanism allowing two transition states, TS type I or TS type II (Figure 11 and Supporting Information); further calculations of the transition state consider only the inversion mechanism.

In case of the lowest-energy identified transition states, an interesting aspect was that compound **1e** presented a TS type II, which showed a linear arrangement of the azo group and neighboring pyrazole carbon atom, whereas compound **1i** had a TS type I (similar linear geometry involving neighboring aryl carbon), which is what is usually found for this kind of azopyrazole derivatives. The NCI surfaces (Figure 10) clearly showed fewer stabilizing effects in TS-**1e** than in TS-**1i**, and this was most probably the cause for the high values of the half-lives in the bis(trifluoromethyl)azopyrazoles, also considering the higher energy of the transition state for **1e**.

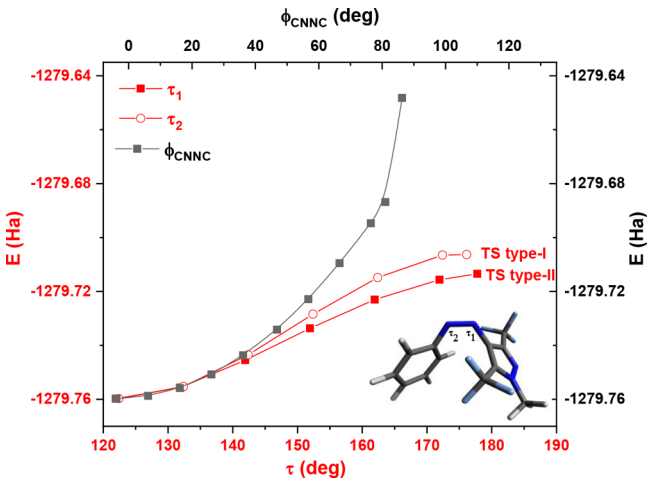

Figure 11. Energy diagram for surface scan of compound **1e**, using scanned variables: the dihedral angle ϕ_{CNNC} corresponding to a rotation mechanism, and angles τ_1 and τ_2 corresponding to two possible inversion mechanisms.

To rationalize the preference of compound **1e** for TS type II, the molecular electrostatic potential (MEP) surface analysis was performed for the *Z* isomers (Figure 12a,b). The highest electron density for compound **1e** was on the nitrogen atom neighboring the pyrazole ring ($q_{N\text{-pyrazole}}$ = −0.125, $q_{N\text{-aryl}}$ = −0.084), while for **1i** the highest electron density was on the nitrogen atom neighboring the aryl ring ($q_{N\text{-pyrazole}}$ = −0.131, $q_{N\text{-aryl}}$ = −0.160). This difference was most likely caused by the presence of the electron-withdrawing trifluoromethyl groups which allowed better accommodation of the excess electron density in the preferred TS type II. This was further sustained by natural bonding orbital (NBO) analysis of compound **1e** (Figure 12). A comparison of TS type I and TS type II clearly showed a higher n−π* stabilizing effect in the case of the latter (Figure 12c,d).

For *Z*−*E* back-isomerization kinetics and the determination of the theoretical half-life values, we considered all *Z* isomers and their corresponding transition states, and the results are described in Table 3 (see Supporting Information for details regarding the method of calculation of half-lives). The calculated N═N Wiberg index and the azo bond length in the *Z* form correlate well, as previously proposed by Fuchter et al.:[24] the shorter the azo bond is, the larger the Wiberg index is, generating a higher activation energy and hence a longer half-life. We could observe a very good correlation of the calculated half-lives with the experimental values, in terms of range and differences between compounds.

CONCLUSIONS

In conclusion, we described herein the synthesis of novel arylazopyrazoles, designed to study the influence of the trifluoromethyl group as well as of other electron-donating and -withdrawing substituted aryl groups grafted on the heterocycle moiety, on the photoswitching behavior of these compounds. The synthesis occurred with reasonable overall yields after two or three reaction steps and involved initial formation of hydrazones. Further, we performed UV−vis and NMR experiments to determine the photoswitching parameters: addressability, fatigue resistance, thermal stability, and efficiency. We found that the novel compounds displayed an excellent fatigue resistance and, more importantly, our arylazo-

https://doi.org/10.1021/acsomega.2c04984
ACS Omega 2022, 7, 39122−39135

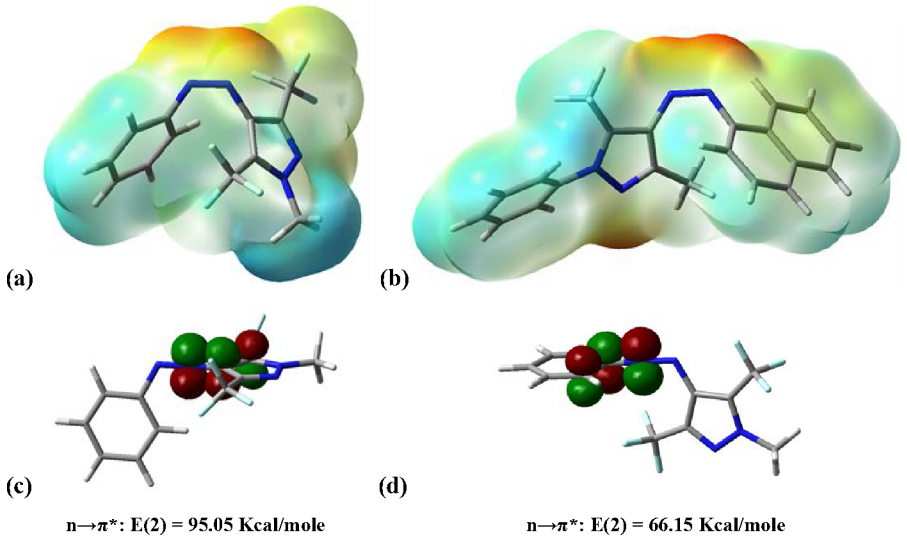

Figure 12. Molecular electrostatic potential (MEP) surfaces generated for compounds **1e** (a) and **1i** (b). High electron density regions are marked with red, whereas low electron density ones are in blue. Natural bonding orbital (NBO) analysis for TS type I (d) and TS type II (c) of compound **1e** (for compound **1i** see Supporting Information).

Table 3. Structural Parameters Associated with *Z*−*E* Back-isomerization Kinetics

compd	TS type	$q_{N\text{-pyrazole}}$	$q_{N\text{-aryl}}$	N=N Wiberg index	N=N bond (Å)	calcd $t_{1/2}$ (h)	exptl $t_{1/2}$ (h)
1e	II	−0.125	−0.084	1.9376	1.240	1046.5	3504
1i	I	−0.131	−0.160	1.8713	1.247	38.8	12.9

1*H*-3,5-ditrifluoromethylpyrazoles displayed very long half-lives in DMSO, in the days range. The presence of the fluorine atoms did not significantly enhance the separation bands compared to previously reported dimethyl-substituted derivatives, but it is reasonable enough to ensure PSS values over 70%. Inclusion into the structure of the compounds of moieties such as 1-naphthyl or 2-naphthyl was beneficial only in combination with the trifluoromethyl-derived compounds, while extending the conjugation onto the pyrazole moiety with electron-donating or -withdrawing substituents positively affected the photoswitching behavior, in terms of isomerization yield and half-lives of the least stable isomer. The experimental trends in stability and half-life were sustained by DFT calculations. One can note that systematic investigation of such compounds is further required in order to fine-tune the structural particularities required to balance the values of the photoswitching parameters. This is strongly related to the desired application and the need to focus on the decisive parameter, and the herein reported compounds cover a wide window in terms of variability of the photoswitching parameters.

EXPERIMENTAL SECTION

General Experimental Information. All reagents and solvents were purchased from commercial suppliers and used without further purification. Thin-layer chromatography (TLC) was performed on silica gel coated aluminum F254 plates. All plates were visualized by UV irradiation at 254 nm. High-resolution mass spectra were recorded on a Thermo Scientific (LTQ XL Orbitrap) spectrometer using the APCI technique in positive ion mode. Melting points were determined in open capillary tubes using a STUART SMP3 electric melting point apparatus and are uncorrected. The irradiation experiments were realized using a 254/365 UV lamp for thin-layer chromatography and an Asahi Spectra's MAX-303 xenon light source with the corresponding band-pass filters, 365 and 450 nm, respectively. Absorption spectra were recorded on a Jasco V-630 spectrophotometer using a 10 mm quartz cell.

Crystallography. X-ray diffraction measurements for crystals **3bH**, **3cF**, **1i**, **1l**, **1o**, and **1n** were performed on a Rigaku XtaLAB Synergy-S diffractometer operating with a Mo Kα (λ = 0.71073 Å) microfocus sealed X-ray tube. The structures were solved by direct methods and refined by full-matrix least-squares techniques based on F^2. The non-H atoms were refined with anisotropic displacement parameters. Calculations were performed using SHELX-2014 or SHELX-2018 crystallographic software package. A summary of the crystallographic data and the structure refinement details for crystals **3bH**, **3cF**, **1i**, **1l**, **1o**, and **1n** are given in Tables S5 and S6. For the refinement of the disordered CF_3 group in the crystal **3cF** were used geometrical restraints. CCDC reference numbers: 2189252−2189257.

*General Experimental Procedure for Synthesis of Derivatives **1a,c,d**.* A mixture of each corresponding derivative **3** (2 mmol, 1 equiv) and EtOH (10 mL) was stirred at rt until a clear solution was obtained. Aqueous solution of 80% $N_2H_4 \cdot H_2O$ (0.3 mL, 7.7 mmol, 3.9 equiv) was added dropwise, and the mixture was refluxed until complete consumption of the starting material, as monitored by TLC. The reaction crude was cooled to rt, precipitated with distilled water (100 mL), and filtered. The product was purified by recrystallization from EtOH/H_2O, filtered, washed with water, and dried.

*(E)-3,5-Bis(trifluoromethyl)-4-(phenyldiazenyl)-1H-pyrazole (**1a**).* Recrystallized from toluene/heptane. Yellow solid. Yield 73% (0.58 g). Mp 186−188 °C. R_f = 0.15 (AcOEt:heptane = 3:7). ^{1}H NMR (500 MHz, DMSO-d_6) δ 7.81 (m, 2H, H_{Ar}), 7.62 (overlapped peaks, 3H, H_{Ar}), 3.37 (bs, 1H, N*H*). ^{13}C NMR (125 MHz, DMSO-d_6) δ 151.8, 134.4, 132.7, 129.72, 129.7, 122.4, 119.9 (q, $^1J_{C-F}$ = 267.9 Hz).

*(E)-3,5-Dimethyl-4-(naphthalen-2-yldiazenyl)-1H-pyrazole (**1c**).* Brick-red solid. Yield 65% (0.32 g). Mp 186−187

https://doi.org/10.1021/acsomega.2c04984
ACS Omega 2022, 7, 39122−39135

°C. R_f = 0.11 (AcOEt:petroleum ether = 1:3). ^{1}H NMR (500 MHz, DMSO-d_6) δ 12.88 (s, 1H, N*H*), 8.31 (d, J = 1.89 Hz, 1H, H_{Ar}), 8.10 (m, 1H, H_{Ar}), 8.00−7.92 (overlapped peaks, 3H, H_{Ar}), 7.57 (overlapped peaks, 2H, H_{Ar}), 2.56 (s, 3H, C*H*$_3$), 2.46 (s, 3H, C*H*$_3$) ppm. ^{13}C NMR (125 MHz, DMSO-d_6) δ 150.6, 142.6, 138.6, 134.3, 133.5, 133.3, 129.0, 128.9, 127.8, 127.0, 126.8, 125.0, 116.5, 13.8, 10.1 ppm. HRMS (APCI+) m/z: calcd for $C_{15}H_{15}N_4$, 251.1297 ([M + H]$^+$, 100%); found 251.1292.

*(E)-3,5-Bis(trifluoromethyl)-4-(naphthalen-2-yldiazenyl)-1H-pyrazole (**1d**).* In this case, the synthesis was performed using 0.55 mmol of hydrazone, and $N_2H_4{\cdot}H_2O$ solution (3.9 equiv) was added dropwise at 0 °C. Then, the mixture stirred at rt. The workup was also changed: After precipitation, the reaction mixture was extracted with AcOEt (3 × 10 mL), and the accumulated organic fractions were further washed with brine and dried over Na_2SO_4; the solvent was evaporated at reduced pressure providing a red residue. The residue was purified by recrystallization in EtOH/H_2O, filtered, washed with water, washed with heptane, and then dried. Yellow solid. Yield 41% (80 mg). Mp 233−235 °C. R_f = 0.53 (AcOEt:petroleum ether = 1:3). ^{1}H NMR (500 MHz, DMSO) δ 8.53 (d, J = 1.96 Hz, 1H, H_{Ar}), 8.25 (m, 1H, H_{Ar}), 8.09 (d, J = 8.92 Hz, 1H, H_{Ar}), 8.04 (dd, J = 7.59, 1.69 Hz, 1H, H_{Ar}), 7.88 (dd, J = 8.90, 1.99 Hz, 1H, H_{Ar}), 7.67 (m, 2H, H_{Ar}) ppm. ^{13}C NMR (125 MHz, DMSO-d_6) δ 149.5, 134.9, 134.5, 132.9, 129.8, 129.7, 129.6, 129.57, 128.7, 127.9, 127.4, 120.0 (q, $^1J_{C-F}$ = 272.6 Hz), 114.6 ppm. HRMS (APCI+) m/z: calcd for $C_{15}H_9F_6N_4$, 359.0726 ([M + H]$^+$, 100%); found 359.0718.

*General Experimental Procedure for Synthesis of Derivatives **1** Using Arylhydrazine Derivatives.* A mixture of each corresponding compound **3** (2 mmol, 1 equiv), arylhydrazine (10.2 mmol, 5.1 equiv), and AcOH (4 mL) and EtOH (10 mL) was stirred at rt until a clear solution was obtained. The mixture was refluxed until complete consumption of the starting material, as monitored by TLC. The crude was then left to cool at rt and concentrated under reduced pressure. The residue was purified by recrystallization in EtOH/H_2O, filtered, washed with water, and dried.

*General Experimental Procedure for the Synthesis of Arylazopyrazole Derivatives **1d,e**.*[35] A mixture of each corresponding derivative **3** (0.39 mmol, 1 equiv), 2,4-dinitrophenylhydrazine (2 mmol, 5.1 equiv), concentrated H_2SO_4 (0.3 mL), AcOH (1 mL), and EtOH (8 mL) was stirred at room temperature until a clear solution was obtained. The mixture was then brought to reflux and left to stir until consumption of the starting material, as monitored by TLC. The mixture was left to cool to room temperature and concentrated under reduced pressure. The residue was purified by recrystallization in DMSO/H_2O, filtered, washed with water, and dried.

General Experimental Procedure for the Synthesis of Arylhydrazine Hydrochloride Derivatives.[36] A mixture of aromatic amine (20.0 mmol, 1 equiv) and AcOH (10 mL) was stirred at room temperature until a clear solution was obtained. The mixture was cooled at 0 °C, and concentrated HCl (50 mL) was added dropwise to form a suspension. An aqueous solution of $NaNO_2$ (1.38 g, 20 mmol, 1.0 equiv) in the minimum amount of water (4 mL) was then added dropwise facilitating in situ formation of the corresponding diazonium salt. The reaction mixture was left stirring for 1 h at 0 °C. Then a solution of $SnCl_2{\cdot}2H_2O$ (10 g, 44.3 mmol) in concentrated HCl (10 mL) was added dropwise with vigorous stirring. The resulting suspension was left stirring for 1 h at rt, and the product was filtered and washed with brine, cold water, and cold Et_2O. The resulting product was used without further purification.

*General Experimental Procedure for Synthesis of Derivatives **1i−o** Using Arylhydrazine Hydrochloride Derivatives.* A mixture of each corresponding derivative **3** (0.79 mmol, 1 equiv), arylhydrazine hydrochloride derivative previously prepared (7.9 mmol, 10 equiv), and EtOH (10 mL) was brought to reflux and left to stir until consumption of the starting material, as monitored by TLC. Water (100 mL) was added resulting in a precipitate. The reaction mixture was extracted with AcOEt (3 × 10 mL), and the combined organic fractions were further washed with brine and dried over Na_2SO_4; the solvent was further removed under reduced pressure. The residue was purified by recrystallization in EtOH/H_2O, filtered, washed with water, and dried.

*(E)-3,5-Dimethyl-1-phenyl-4-(naphthalen-1-yldiazenyl)-1H-pyrazole (**1i**).* Orange solid. Yield 72% (0.46 g). Mp 131−132 °C. R_f = 0.69 (AcOEt:petroleum ether = 1:3). ^{1}H NMR (500 MHz, DMSO-d_6) δ 8.74 (d, J = 8.40 Hz, 1H, H_{Ar}), 8.05 (d, J = 8.17 Hz, 1H, H_{Ar}), 8.05 (d, J = 8.29 Hz, 1H, H_{Ar}), 7.79 (d, J = 7.48 Hz, 1H, H_{Ar}), 7.71 (m, 1H, H_{Ar}), 7.65 (overlapped peaks, 4H, H_{Ar}), 7.59 (overlapped peaks, 2H, H_{Ar}), 7.50 (t, J = 7.37 Hz, 1H, H_{Ar}), 2.73 (s, 3H, C*H*$_3$), 2.62 (s, 3H, C*H*$_3$) ppm. ^{13}C NMR (125 MHz, DMSO-d_6) δ 147.8, 142.0, 140.6, 138.6, 136.7, 134.0, 130.2, 130.0, 129.4, 128.2, 128.1, 127.0, 126.5, 125.9, 124.6, 122.8, 110.7, 14.5, 11.1 ppm. HRMS (APCI+) m/z calcd for $C_{21}H_{19}N_4$, 327.1604 ([M + H]$^+$, 100%); found 327.1613.

*(E)-3,5-Dimethyl-1-(2,4-dinitrophenyl)-4-(naphthalen-1-yldiazenyl)-1H-pyrazole (**1j**).* Red solid. Yield 49% (80 mg). Mp 228−229 °C. R_f = 0.47 (AcOEt:petroleum ether = 1:3). ^{1}H NMR (500 MHz, DMSO-d_6) δ 8.97 (d, J = 2.56 Hz, 1H, H_{Ar}), 8.74 (overlapped peaks, 2H, H_{Ar}), 8.28 (d, J = 8.73 Hz, 1H, H_{Ar}), 8.10 (d, J = 8.11 Hz, 1H, H_{Ar}), 8.07 (m, 1H, H_{Ar}), 7.82 (dd, J = 7.54, 1.12 Hz, 1H, H_{Ar}), 7.72 (ddd, J = 8.35, 6.78, 1.37 Hz, 1H, H_{Ar}), 7.66 (overlapped peaks, 2H, H_{Ar}), 2.74 (s, 3H, C*H*$_3$), 2.57 (s, 3H, C*H*$_3$) ppm. ^{13}C NMR (125 MHz, DMSO-d_6) δ 147.7, 147.0, 145.4, 144.4, 142.1, 136.8, 135.4, 134.0, 130.6, 130.2, 129.8, 129.7, 128.4, 128.1, 127.2, 126.6, 125.9, 121.4, 111.0, 14.4, 10.4 ppm. HRMS (APCI+) m/z: calcd for $C_{21}H_{17}N_6O_4$, 417.1306 ([M + H]$^+$, 100%); found 417.1296.

*(E)-3,5-Dimethyl-1-(p-tolyl)-4-(naphthalen-1-yldiazenyl)-1H-pyrazole (**1k**).* Yellow solid. Yield 52% (0.14 g). Mp 123−124 °C. R_f = 0.77 (AcOEt:petroleum ether = 1:3). ^{1}H NMR (500 MHz, DMSO-d_6) δ 8.74 (m, 1H, H_{Ar}), 8.05 (overlapped peaks, 2H, H_{Ar}), 7.78 (dd, J = 7.55, 1.11 Hz, 1H, H_{Ar}), 7.70 (ddd, J = 8.31, 6.78, 1.33 Hz, 1H, H_{Ar}), 7.64 (overlapped peaks, 2H, H_{Ar}), 7.52 (m, 2H, H_{Ar}), 7.39 (m, 2H, H_{Ar}), 2.70 (s, 3H, pyrazole-C*H*$_3$), 2.61 (s, 3H, pyrazole-C*H*$_3$), 2.40 (s, 3H, tolyl-C*H*$_3$) ppm. ^{13}C NMR (125 MHz, DMSO-d_6) δ 147.8, 141.9, 140.3, 137.7, 136.5, 136.2, 133.9, 130.1, 129.8, 129.7, 128.0, 126.9, 126.5, 125.9, 124.5, 122.8, 110.7, 20.6, 14.4, 11.0 ppm. HRMS (APCI+) m/z: calcd for $C_{22}H_{21}N_4$, 341.1766 ([M + H]$^+$, 100%); found 341.1765.

*(E)-3,5-Dimethyl-1-phenyl-4-(naphthalen-2-yldiazenyl)-1H-pyrazole (**1l**).* Orange solid. Yield 79% (0.51 g). Mp 123−124 °C. R_f = 0.65 (AcOEt:petroleum ether = 1:3). ^{1}H NMR (500 MHz, DMSO-d_6) δ 8.40 (s, 1H, H_{Ar}), 8.13 (m, 1H, H_{Ar}), 8.04−7.97 (overlapped peaks, 3H, H_{Ar}), 7.64 (overlapped

https://doi.org/10.1021/acsomega.2c04984
ACS Omega 2022, 7, 39122−39135

peaks, 2H, H_{Ar}), 7.60 (overlapped peaks, 4H, H_{Ar}), 7.49 (t, J = 7.30 Hz, 1H, H_{Ar}), 2.70 (s, 3H, CH_3), 2.55 (s, 3H, CH_3) ppm. ^{13}C NMR (125 MHz, DMSO-d_6) δ 150.5, 142.2, 140.0, 138.7, 135.6, 133.7, 133.3, 129.3, 129.2, 128.9, 128.1, 127.8, 127.2, 126.9, 125.6, 124.6, 116.4, 14.1, 11.0 ppm. HRMS (APCI+) m/z: calcd for $C_{21}H_{19}N_4$, 327.1604 ([M + H]$^+$, 100%); found 327.1615.

*(E)-3,5-Dimethyl-1-(2,4-dinitrophenyl)-4-(naphthalen-2-yldiazenyl)-1H-pyrazole (**1m**).* Red solid. Yield 51% (83 mg). Mp 176−178 °C. R_f = 0.50 (AcOEt:petroleum ether = 1:3). ^{1}H NMR (500 MHz, DMSO-d_6) δ 8.96 (d, J = 2.55 Hz, 1H, H_{Ar}), 8.73 (dd, J = 8.74, 2.58 Hz, 1H, H_{Ar}), 8.45 (d, J = 1.94 Hz, 1H, H_{Ar}), 8.26 (d, J = 8.72 Hz, 1H, H_{Ar}), 8.15 (m, 1H, H_{Ar}), 8.05 (d, J = 8.93 Hz, 1H, H_{Ar}), 8.01 (overlapped peaks, 2H, H_{Ar}), 7.62 (overlapped peaks, 2H, H_{Ar}), 2.71 (s, 3H, CH_3), 2.50 (overlap with solvent peak, CH_3) ppm. ^{13}C NMR (125 MHz, DMSO-d_6) δ 150.3, 147.0, 145.4, 144.7, 141.4, 135.8, 135.5, 134.0, 133.2, 129.7, 129.2, 128.4, 127.9, 127.5, 127.0, 126.3, 126.0, 121.3, 116.1, 14.0, 10.4 ppm. HRMS (APCI+) m/z: calcd for $C_{21}H_{17}N_6O_4$, 417.1306 ([M + H]$^+$, 100%); found 417.1295.

*(E)-3,5-Dimethyl-1-(p-tolyl)-4-(naphthalen-2-yldiazenyl)-1H-pyrazole (**1n**).* Yellow solid. Yield 63% (0.17 g). Mp 153−154 °C. R_f = 0.77 (AcOEt:petroleum ether = 1:3). ^{1}H NMR (500 MHz, DMSO-d_6) δ 8.38 (m, 1H, H_{Ar}), 8.12 (m, 1H, H_{Ar}), 8.00 (overlapped peaks, 3H, H_{Ar}), 7.59 (overlapped peaks, 2H, H_{Ar}), 7.50 (m, 2H, H_{Ar}), 7.38 (d, J = 8.27 Hz, 2H, H_{Ar}), 2.67 (s, 3H, pyrazole-CH_3), 2.54 (s, 3H, pyrazole-CH_3), 2.40 (s, 3H, tolyl-CH_3). ^{13}C NMR (125 MHz, DMSO-d_6) δ 150.5, 142.0, 139.7, 137.7, 136.2, 135.5, 133.7, 133.3, 129.7, 129.1, 129.0, 127.8, 127.1, 126.8, 125.4, 125.0, 124.4, 116.4, 20.6, 14.0, 11.0 ppm. HRMS (APCI+) m/z: calcd for $C_{22}H_{21}N_4$, 341.1766 ([M + H]$^+$, 100%); found 341.1762.

*(E)-3,5-Dimethyl-1-(naphthalen-2-yl)-4-(naphthalen-2-yldiazenyl)-1H-pyrazole (**1o**).* Yellow solid. Yield 71% (0.21 g). Mp 190−192 °C. R_f = 0.77 (AcOEt:petroleum ether = 1:3). ^{1}H NMR (500 MHz, DMSO-d_6) δ 8.42 (dd, J = 1.71, 0.87 Hz, 1H), 8.22 (d, J = 2.15 Hz, 1H), 8.13 (dd, J = 9.17, 4.94 Hz, 2H), 8.04 (m, 5H), 7.81 (dd, J = 8.73, 2.19 Hz, 1H), 7.62 (m, 4H), 2.79 (s, 3H, CH_3), 2.59 (s, 3H, CH_3). ^{13}C NMR (125 MHz, DMSO-d_6) δ 150.5, 142.4, 140.3, 136.1, 135.7, 133.7, 133.3, 132.8, 132.0, 129.7, 129.2, 128.2, 127.8, 127.2, 127.1, 126.9, 126.85, 125.6, 125.2, 122.8, 122.5, 122.4, 116.4, 14.2, 11.1 ppm. HRMS (APCI+) m/z: calcd for $C_{25}H_{21}N_4$, 377.1766 ([M + H]$^+$, 100%); found 377.1763.

*General Experimental Procedure for Synthesis of Derivatives **1e**.*[27] A mixture of **3aF** (0.22 mmol, 1 equiv) and DMSO (1 mL) was stirred at room temperature until a clear solution was obtained. Powdered NaOH (26.4 mg, 0.66 mmol, 3 equiv) was added, and the mixture was stirred at 80 °C for 1 h. The reaction was left to cool to rt, and a solution of MeI (39.4 μL, 0.26 mmol, 1.2 equiv) in DMSO (1 mL) was added dropwise. The mixture was left to stir until consumption of the starting material, as monitored by TLC. Water (10 mL) was added, resulting in the formation of a yellow precipitate. The reaction mixture was extracted with AcOEt (3 × 10 mL), and the accumulated organic fractions were further washed with brine and dried over Na_2SO_4; the solvent was further removed under reduced pressure providing a yellow residue. The residue was purified by recrystallization in EtOH/H_2O, filtered, washed with water, and dried.

*General Experimental Procedure for Synthesis of Derivatives **1f−h**.* A suspension of each corresponding derivative **1a−d** (0.4 mmol, 1 equiv) and TBAB (0.02 g, 0.06 mmol, 0.15 equiv) in H_2O (10 mL) was cooled to 0 °C. Powdered KOH (0.15 g, 2.1 mmol, 5.25 equiv) was added and placed in an ultrasound bath for 5 min. MeI (0.2 mL, 3.21 mmol, 8 equiv) was added, and the mixture was stirred at room temperature until consumption of the starting materials, as monitored by TLC. The reaction crude was diluted with H_2O (100 mL) and filtered, and the precipitate was washed with water. The product was purified by recrystallization in EtOH/H_2O, filtered, washed with water, and dried.

*(E)-1-Methyl-3,5-bis(trifluoromethyl)-4-(phenyldiazenyl)-1H-pyrazole (**1e**).* Recrystallized from DMSO/H_2O. Orange solid. Yield 48% (0.11 g). Mp 112−114 °C. R_f = 0.78 (AcOEt:heptane = 3:7). ^{1}H NMR (500 MHz, DMSO-d_6) δ 7.81 (m, 2H, H_{Ar}), 7.63 (overlapped peaks, 3H, H_{Ar}), 4.17 (d, J = 1.5 Hz, 3H, CH_3). ^{13}C NMR (125 MHz, DMSO-d_6) δ 151.7, 135.9, 132.8, 130.0 (q, J = 39.2 Hz), 129.7, 129.2 (q, J = 39.2 Hz), 122.4, 120.3 (q, $^1J_{C-F}$ = 268.5 Hz), 119.0 (q, $^1J_{C-F}$ = 271.4 Hz), 40.8 (q, J = 2.6 Hz) ppm.

*(E)-1,3,5-Trimethyl-4-(naphthalen-1-yldiazenyl)-1H-pyrazole (**1f**).* Orange solid. Yield 45% (47 mg). Mp 119−120 °C. R_f = 0.24 (AcOEt:petroleum ether = 1:3). ^{1}H NMR (500 MHz, DMSO-d_6) δ 8.70 (d, J = 8.37 Hz, 1H, H_{Ar}), 8.02 (overlapped peaks, 2H, H_{Ar}), 7.73 (d, J = 7.46 Hz, 1H, H_{Ar}), 7.68 (t, J = 7.55 Hz, 1H, H_{Ar}), 7.61 (overlapped peaks, 2H, H_{Ar}), 3.78 (s, 3H, NCH_3), 2.63 (s, 3H, CH_3), 2.49 (s, 3H, CH_3) ppm. ^{13}C NMR (125 MHz, DMSO-d_6) δ 147.9, 140.3, 140.2, 135.6, 134.0, 130.1, 129.5, 128.0, 126.8, 126.4, 125.9, 122.8, 110.6, 36.0, 14.3, 9.6 ppm. HRMS (APCI+) m/z: calcd for $C_{16}H_{17}N_4$, 265.14477 ([M + H]$^+$, 100%); found 265.14365.

*(E)-1,3,5-Trimethyl-4-(naphthalen-2-yldiazenyl)-1H-pyrazole (**1g**).* Orange solid. Yield 55% (58 mg). Mp 117−118 °C. R_f = 0.23 (AcOEt:petroleum ether = 1:3). ^{1}H NMR (500 MHz, DMSO-d_6) δ 8.31 (s, 1H, H_{Ar}), 8.1−7.92 (overlapped peaks, 4H, H_{Ar}), 7.57 (overlapped peaks, 2H, H_{Ar}), 3.76 (s, 3H, NCH_3), 2.60 (s, 3H, CH_3), 2.43 (s, 3H, CH_3) ppm. ^{13}C NMR (125 MHz, DMSO-d_6) δ 150.5, 140.4, 139.6, 134.5, 133.5, 133.3, 129.0, 128.9, 127.8, 127.0, 126.8, 125.0, 116.5, 36.0, 13.9, 9.5 ppm. HRMS (APCI+) m/z: calcd for $C_{16}H_{17}N_4$, 265.14477 ([M + H]$^+$, 100%); found 265.14353.

*(E)-1-Methyl-3,5-bis(trifluoromethyl)-4-(naphthalen-2-yldiazenyl)-1H-pyrazole (**1h**).* Recrystallized from DMSO/H_2O. Yellow solid. Yield 66% (65 mg). Mp 118−120 °C. R_f = 0.83 (AcOEt:petroleum ether = 1:3). ^{1}H NMR (500 MHz, DMSO-d_6) δ 8.53 (d, J = 2.01 Hz, 1H, H_{Ar}), 8.24 (dd, J = 7.79, 1.68 Hz, 1H, H_{Ar}), 8.07 (d, J = 8.94 Hz, 1H, H_{Ar}), 8.03 (dd, J = 7.82, 1.61 Hz, 1H, H_{Ar}), 7.86 (dd, J = 8.90, 2.00 Hz, 1H, H_{Ar}), 7.67 (overlapped peaks, 2H, H_{Ar}), 4.18 (d, J = 1.55 Hz, 3H, CH_3) ppm. ^{13}C NMR (125 MHz, DMSO-d_6) δ 149.4, 136.0, 134.9, 132.9, 130.1, 129.8, 129.3, 129.0, 128.7, 127.9, 127.4, 121.4, 120.37 (d, J = 268.97 Hz), 119.07 (d, J = 271.08 Hz), 114.6, 40.8 ppm. HRMS (APCI+) m/z: calcd for $C_{16}H_{11}F_6N_4$, 373.0888 ([M + H]$^+$, 100%); found 373.0887.

■ ASSOCIATED CONTENT

Supporting Information

The Supporting Information is available free of charge at https://pubs.acs.org/doi/10.1021/acsomega.2c04984.

https://doi.org/10.1021/acsomega.2c04984
ACS Omega 2022, 7, 39122−39135

^{1}H NMR spectra for all compounds, additional experimental details, XRD data analysis, absorption spectroscopy, computational analysis, and HRMS (PDF)

CIF data (ZIP)

AUTHOR INFORMATION

Corresponding Author

Mihaela Matache − *Research Centre of Applied Organic Chemistry, Department of Organic Chemistry, Biochemistry and Catalysis, Faculty of Chemistry, University of Bucharest, 050663 Bucharest, Romania;* orcid.org/0000-0001-7956-7162; Email: mihaela.matache@g.unibuc.ro

Authors

Bogdan C. Enache − *Research Centre of Applied Organic Chemistry, Department of Organic Chemistry, Biochemistry and Catalysis, Faculty of Chemistry, University of Bucharest, 050663 Bucharest, Romania; Department of Research and Development, SC Microsin SRL, 032364 Bucharest, Romania*

Anamaria Hanganu − *Research Centre of Applied Organic Chemistry, Department of Organic Chemistry, Biochemistry and Catalysis, Faculty of Chemistry, University of Bucharest, 050663 Bucharest, Romania; "C. D. Nenitzescu" Institute of Organic and Supramolecular Chemistry of the Romanian Academy, 060023 Bucharest, Romania*

Cristina Tablet − *Faculty of Pharmacy, Titu Maiorescu University, 040317 Bucharest, Romania; Department of Physical Chemistry, University of Bucharest, 030018 Bucharest, Romania*

Catalin C. Anghel − *Research Centre of Applied Organic Chemistry, Department of Organic Chemistry, Biochemistry and Catalysis, Faculty of Chemistry, University of Bucharest, 050663 Bucharest, Romania; Supramolecular Organic and Organometallic Chemistry Centre, Faculty of Chemistry and Chemical Engineering, "Babes−Bolyai" University, 400028 Cluj-Napoca, Romania;* orcid.org/0000-0001-5540-4158

Codruta C. Popescu − *Research Centre of Applied Organic Chemistry, Department of Organic Chemistry, Biochemistry and Catalysis, Faculty of Chemistry, University of Bucharest, 050663 Bucharest, Romania*

Anca Paun − *Research Centre of Applied Organic Chemistry, Department of Organic Chemistry, Biochemistry and Catalysis, Faculty of Chemistry, University of Bucharest, 050663 Bucharest, Romania*

Niculina Daniela Hădade − *Supramolecular Organic and Organometallic Chemistry Centre, Faculty of Chemistry and Chemical Engineering, "Babes−Bolyai" University, 400028 Cluj-Napoca, Romania;* orcid.org/0000-0001-5882-5759

Augustin M. Mădălan − *Inorganic Chemistry Department, Faculty of Chemistry, University of Bucharest, 030018 Bucharest, Romania*

Complete contact information is available at: https://pubs.acs.org/10.1021/acsomega.2c04984

Notes

The authors declare no competing financial interest.

ACKNOWLEDGMENTS

This work was supported by a grant of the Romanian Ministry of Education and Research, CNCS-UEFISCDI, project number PN-III-P1-1.1-TE-2019-1003, within PNCDI III. The University of Bucharest-UniRem project no. 244 is also gratefully acknowledged. We are grateful to Dr. Mihaela Florea for access to the irradiation instrument.

REFERENCES

(1) Yang, Z.; Liu, Z.; Yuan, L. Recent Advances of Photoresponsive Supramolecular Switches. *Asian J. Org. Chem.* **2021**, *10* (1), 74−90.

(2) Danowski, W.; van Leeuwen, T.; Browne, W. R.; Feringa, B. L. Photoresponsive Porous Materials. *Nanoscale Adv.* **2021**, *3* (1), 24−40.

(3) Pianowski, Z. L. Recent Implementations of Molecular Photoswitches into Smart Materials and Biological Systems. *Chem. - A Eur. J.* **2019**, *25* (20), 5128−5144.

(4) Goulet-Hanssens, A.; Eisenreich, F.; Hecht, S. Enlightening Materials with Photoswitches. *Adv. Mater.* **2020**, *32* (20), 1905966.

(5) Fuchter, M. J. On the Promise of Photopharmacology Using Photoswitches: A Medicinal Chemist's Perspective. *J. Med. Chem.* **2020**, *63* (20), 11436−11447.

(6) Welleman, I. M.; Hoorens, M. W. H.; Feringa, B. L.; Boersma, H. H.; Szymański, W. Photoresponsive Molecular Tools for Emerging Applications of Light in Medicine. *Chem. Sci.* **2020**, *11* (43), 11672−11691.

(7) Volarić, J.; Szymanski, W.; Simeth, N. A.; Feringa, B. L. Molecular Photoswitches in Aqueous Environments. *Chem. Soc. Rev.* **2021**, *50* (22), 12377−12449.

(8) Dong, L.; Feng, Y.; Wang, L.; Feng, W. Azobenzene-Based Solar Thermal Fuels: Design, Properties, and Applications. *Chem. Soc. Rev.* **2018**, *47* (19), 7339−7368.

(9) She, P.; Qin, Y.; Wang, X.; Zhang, Q. Recent Progress in External-Stimulus-Responsive 2D Covalent Organic Frameworks. *Adv. Mater.* **2022**, *34* (22), 2101175.

(10) Yu, F.; Liu, W.; Li, B.; Tian, D.; Zuo, J.; Zhang, Q. Photostimulus-Responsive Large-Area Two-Dimensional Covalent Organic Framework Films. *Angew. Chemie Int. Ed.* **2019**, *58* (45), 16101−16104.

(11) Hsu, C.-W.; Sauvée, C.; Sundén, H.; Andréasson, J. Writing and Erasing Multicolored Information in Diarylethene-Based Supramolecular Gels. *Chem. Sci.* **2018**, *9* (41), 8019−8023.

(12) Hvilsted, Sør.; Sanchez, C.; Alcala, R. The Volume Holographic Optical Storage Potential in Azobenzene Containing Polymers. *J. Mater. Chem.* **2009**, *19* (37), 6641.

(13) Liu, Z.; Ren, S.; Guo, X. Switching Effects in Molecular Electronic Devices. *Top. Curr. Chem.* **2017**, *375* (3), 56.

(14) Velema, W. A.; Szymanski, W.; Feringa, B. L. Photopharmacology: Beyond Proof of Principle. *J. Am. Chem. Soc.* **2014**, *136* (6), 2178−2191.

(15) Broichhagen, J.; Frank, J. A.; Trauner, D. A Roadmap to Success in Photopharmacology. *Acc. Chem. Res.* **2015**, *48* (7), 1947−1960.

(16) Knie, C.; Utecht, M.; Zhao, F.; Kulla, H.; Kovalenko, S.; Brouwer, A. M.; Saalfrank, P.; Hecht, S.; Bléger, D. Ortho -Fluoroazobenzenes: Visible Light Switches with Very Long-Lived Z Isomers. *Chem. - A Eur. J.* **2014**, *20* (50), 16492−16501.

(17) Weston, C. E.; Richardson, R. D.; Haycock, P. R.; White, A. J. P. P.; Fuchter, M. J. Arylazopyrazoles: Azoheteroarene Photoswitches Offering Quantitative Isomerization and Long Thermal Half-Lives. *J. Am. Chem. Soc.* **2014**, *136* (34), 11878−11881.

(18) Crespi, S.; Simeth, N. A.; König, B. Heteroaryl Azo Dyes as Molecular Photoswitches. *Nat. Rev. Chem.* **2019**, *3* (3), 133−146.

(19) Ren, H.; Yang, P.; Winnik, F. M. Azopyridine: A Smart Photo- and Chemo-Responsive Substituent for Polymers and Supramolecular Assemblies. *Polym. Chem.* **2020**, *11* (37), 5955−5961.

(20) Balam-Villarreal, J. A.; López-Mayorga, B. J.; Gallardo-Rosas, D.; Toscano, R. A.; Carreón-Castro, M. P.; Basiuk, V. A.; Cortés-

Guzmán, F.; López-Cortés, J. G.; Ortega-Alfaro, M. C. π-Extended Push-Pull Azo-Pyrrole Photoswitches: Synthesis, Solvatochromism and Optical Band Gaps. *Org. Biomol. Chem.* **2020**, *18* (8), 1657−1670.
(21) Wendler, T.; Schütt, C.; Näther, C.; Herges, R. Photoswitchable Azoheterocycles via Coupling of Lithiated Imidazoles with Benzenediazonium Salts. *J. Org. Chem.* **2012**, *77* (7), 3284−3287.
(22) Crespi, S.; Simeth, N. A.; Bellisario, A.; Fagnoni, M.; König, B. Unraveling the Thermal Isomerization Mechanisms of Heteroaryl Azoswitches: Phenylazoindoles as Case Study. *J. Phys. Chem. A* **2019**, *123* (9), 1814−1823.
(23) Kennedy, A. D. W.; Sandler, I.; Andréasson, J.; Ho, J.; Beves, J. E. Visible-Light Photoswitching by Azobenzazoles. *Chem. - A Eur. J.* **2020**, *26* (5), 1103−1110.
(24) Calbo, J.; Weston, C. E.; White, A. J. P.; Rzepa, H. S.; Contreras-Garcia, J.; Fuchter, M. J. Tuning Azoheteroarene Photoswitch Performance through Heteroaryl Design. *J. Am. Chem. Soc.* **2017**, *139* (3), 1261−1274.
(25) Rustler, K.; Nitschke, P.; Zahnbrecher, S.; Zach, J.; Crespi, S.; König, B. Photochromic Evaluation of 3(5)-Arylazo-1 H-Pyrazoles. *J. Org. Chem.* **2020**, *85* (6), 4079−4088.
(26) Calbo, J.; Thawani, A. R.; Gibson, R. S. L.; White, A. J. P.; Fuchter, M. J. A Combinatorial Approach to Improving the Performance of Azoarene Photoswitches. *Beilstein J. Org. Chem.* **2019**, *15*, 2753−2764.
(27) Devi, S.; Saraswat, M.; Grewal, S.; Venkataramani, S. Evaluation of Substituent Effect in Z -Isomer Stability of Arylazo-1 H −3,5-Dimethylpyrazoles: Interplay of Steric, Electronic Effects and Hydrogen Bonding. *J. Org. Chem.* **2018**, *83* (8), 4307−4322.
(28) Stricker, L.; Böckmann, M.; Kirse, T. M.; Doltsinis, N. L.; Ravoo, B. J. Arylazopyrazole Photoswitches in Aqueous Solution: Substituent Effects, Photophysical Properties, and Host-Guest Chemistry. *Chem. - A Eur. J.* **2018**, *24* (34), 8639−8647.
(29) Adam, V.; Prusty, D. K.; Centola, M.; Škugor, M.; Hannam, J. S.; Valero, J.; Klöckner, B.; Famulok, M. Expanding the Toolbox of Photoswitches for DNA Nanotechnology Using Arylazopyrazoles. *Chem. - A Eur. J.* **2018**, *24* (5), 1062−1066.
(30) Dwyer, B. G.; Wang, C.; Abegg, D.; Racioppo, B.; Qiu, N.; Zhao, Z.; Pechalrieu, D.; Shuster, A.; Hoch, D. G.; Adibekian, A. Chemoproteomics-Enabled De Novo Discovery of Photoswitchable Carboxylesterase Inhibitors for Optically Controlled Drug Metabolism. *Angew. Chemie Int. Ed.* **2021**, *60* (6), 3071−3079.
(31) Weston, C. E.; Kramer, A.; Colin, F.; Yildiz, O.; Baud, M. G. J.; Meyer-Almes, F.-J.; Fuchter, M. J. Toward Photopharmacological Antimicrobial Chemotherapy Using Photoswitchable Amidohydrolase Inhibitors. *ACS Infect. Dis.* **2017**, *3* (2), 152−161.
(32) Xu, X.; Wu, B.; Zhang, P.; Xing, Y.; Shi, K.; Fang, W.; Yu, H.; Wang, G. Arylazopyrazole-Based Dendrimer Solar Thermal Fuels: Stable Visible Light Storage and Controllable Heat Release. *ACS Appl. Mater. Interfaces* **2021**, *13* (19), 22655−22663.
(33) Chu, C.; Stricker, L.; Kirse, T. M.; Hayduk, M.; Ravoo, B. J. Light-Responsive Arylazopyrazole Gelators: From Organic to Aqueous Media and from Supramolecular to Dynamic Covalent Chemistry. *Chem. - A Eur. J.* **2019**, *25* (24), 6131−6140.
(34) Ludwanowski, S.; Skarsetz, O.; Creusen, G.; Hoenders, D.; Straub, P.; Walther, A. Wavelength-Gated Adaptation of Hydrogel Properties via Photo-Dynamic Multivalency in Associative Star Polymers. *Angew. Chemie Int. Ed.* **2021**, *60* (8), 4358−4367.
(35) Garg, H. G.; Singh, P. P. Potential Antidiabetics. I. 1-(2,4-Dinitrophenyl)-3,5-Dimethyl-4-Arylazopyrazoles. *J. Med. Chem.* **1968**, *11* (5), 1103−1104.
(36) Jasch, H.; Scheumann, J.; Heinrich, M. R. Regioselective Radical Arylation of Anilines with Arylhydrazines. *J. Org. Chem.* **2012**, *77* (23), 10699−10706.
(37) Yao, H. C. Azohydrazone Conversion. II. The Coupling of Diazonium Ion with β-Diketones. *J. Org. Chem.* **1964**, *29* (10), 2959−2963.
(38) Gilli, G.; Bellucci, F.; Ferretti, V.; Bertolasi, V. Evidence for Resonance-Assisted Hydrogen Bonding from Crystal-Structure Correlations on the Enol Form of the.Beta.-Diketone Fragment. *J. Am. Chem. Soc.* **1989**, *111* (3), 1023−1028.
(39) Alkorta, I.; Elguero, J.; Mó, O.; Yáñez, M.; Del Bene, J. E. Do Coupling Constants and Chemical Shifts Provide Evidence for the Existence of Resonance-Assisted Hydrogen Bonds? *Mol. Phys.* **2004**, *102* (23−24), 2563−2574.
(40) Chai, J.-D.; Head-Gordon, M. Long-Range Corrected Hybrid Density Functionals with Damped Atom-Atom Dispersion Corrections. *Phys. Chem. Chem. Phys.* **2008**, *10* (44), 6615.
(41) Grimme, S. Semiempirical GGA-Type Density Functional Constructed with a Long-Range Dispersion Correction. *J. Comput. Chem.* **2006**, *27* (15), 1787−1799.
(42) Bandara, H. M. D. D.; Burdette, S. C. Photoisomerization in Different Classes of Azobenzene. *Chem. Soc. Rev.* **2012**, *41* (5), 1809−1825.

https://doi.org/10.1021/acsomega.2c04984
ACS Omega 2022, 7, 39122−39135